ACS Medicinal Chemistry Letters

pubs.acs.org/acsmedchemlett

Letter

Development of Iodinated Indocyanine Green Analogs as a Strategy for Targeted Therapy of Liver Cancer

Sierra C. Marker,[▽] Andres F. Espinoza,[▽] A. Paden King, Sarah E. Woodfield, Roma H. Patel, Kwamena Baidoo, Meredith N. Nix, Larissa Miasiro Ciaramicoli, Young-Tae Chang,* Freddy E. Escorcia,* Sanjeev A. Vasudevan,* and Martin J. Schnermann*

Cite This: *ACS Med. Chem. Lett.* 2023, 14, 1208−1215

Read Online

ACCESS | Metrics & More | Article Recommendations | Supporting Information

ABSTRACT: Liver cancer is one of the leading causes of cancer-related deaths, with a significant increase in incidence worldwide. Novel therapies are needed to address this unmet clinical need. Indocyanine green (ICG) is a broadly used fluorescence-guided surgery (FGS) agent for liver tumor resection and has significant potential for conversion to a targeted therapy. Here, we report the design, synthesis, and investigation of a series of iodinated ICG analogs (I-ICG), which can be used to develop ICG-based targeted radiopharmaceutical therapy. We applied a CRISPR-based screen to identify the solute carrier transporter, OATP1B3, as a likely mechanism for ICG uptake. Our lead I-ICG compound specifically localizes to tumors in mice bearing liver cancer xenografts. This study introduces the chemistry needed to incorporate iodine onto the ICG scaffold and defines the impact of these modifications on key properties, including targeting liver cancer *in vitro* and *in vivo*.

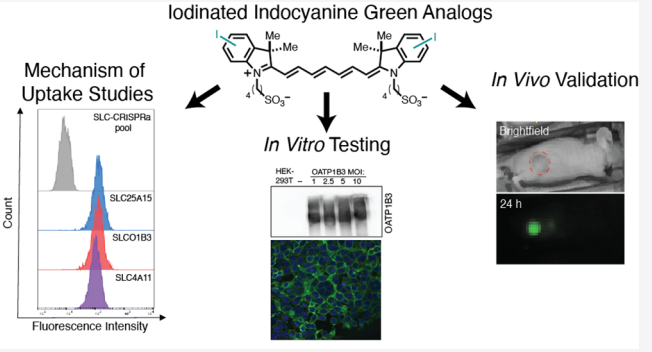

KEYWORDS: *Fluorophore, Fluorescence-guided surgery, Hepatocellular carcinoma, Hepatoblastoma*

Liver cancer is the fourth leading cause of cancer-related deaths around the world, with >1 million people estimated to be affected by 2025.[1] Hepatocellular carcinoma (HCC) makes up 90% of adult liver cancer cases, while hepatoblastoma (HB) is the most common liver malignancy in children, typically occurring between the ages of 6 months and 3 years. HCC, which has five-year survival rates of less than 20%, can also affect teenagers.[2,3] Curative treatment options for early stage HB and HCC include surgical resection, liver transplantation, and local ablation.[4,5] However, most HCC is not detected until advanced stages due to the asymptomatic nature of the disease. For HB, around 60−80% of children have unresectable tumors upon diagnosis, which require treatment with aggressive neoadjuvant chemotherapy regimens.[6] Despite these advances, the lack of an effective targeted therapy for HB and HCC has left physicians subjecting patients to aggressive therapies with deleterious side effects. Thus, there is a significant need for further understanding of ways to create targeted medical therapies toward liver cancer.

Although HB and HCC are unique in their pathophysiology, they both exhibit selective indocyanine green (ICG) uptake, which has proven to be useful for guiding surgical resection. The last two decades have seen significant progress in the development of fluorescence-guided surgery (FGS) approaches for cancer resection.[7−9] The most broadly used FGS probe in the clinic is the near-infrared (NIR)-emitting dye, ICG.[10] ICG was initially used for angiographic imaging for blood flow[11] and then found applications in assessing liver function due to its selective hepatobiliary excretion.[12] Subsequently, it was found that ICG also exhibits remarkably high uptake and retention in liver tumors, as well as other solid tumors.[13−15] ICG is now used broadly to facilitate the resection of HCC tumors in adults and, in recent years, has also been successfully used intraoperatively in HB.[16] Approximately 90% of children with HB exhibit highly ICG-positive tumors, making surgical resection possible in many cases.[17] Due to the dramatic uptake of ICG in both HB and HCC primary and metastatic lesions, an appealing strategy is to repurpose the tumor-targeting property of ICG to selectively deliver a therapeutic agent. Prior efforts have sought to identify ICG derivatives with similar uptake by various types of liver cancer, though these remain in preclinical testing.[18,19] A number of reports demonstrate the potential for ICG small-molecule conjugates for therapy in various cancer types.[20−27] While these reports have illustrated

Received: May 19, 2023
Accepted: August 16, 2023
Published: August 24, 2023

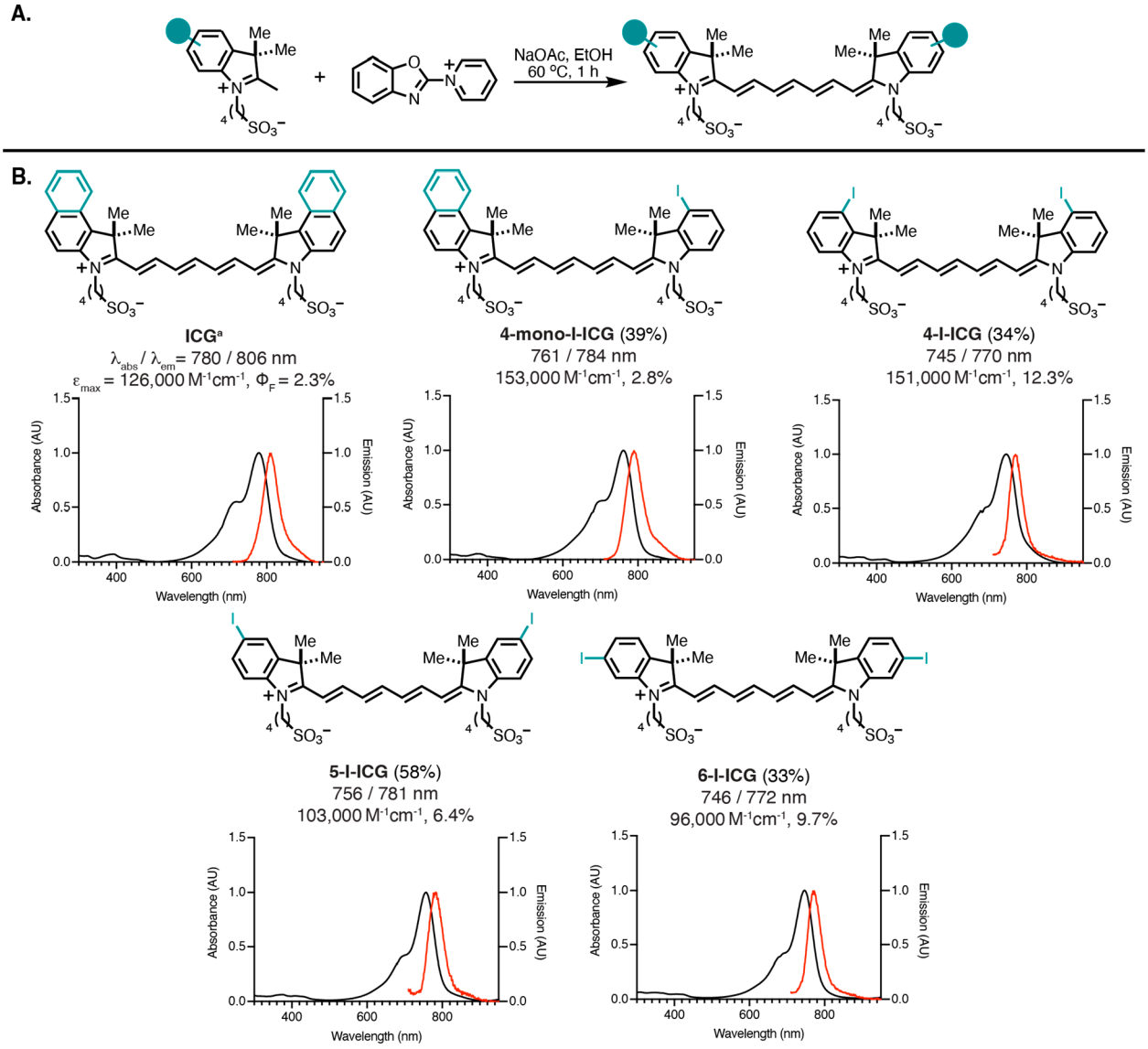

Figure 1. (A) Synthesis of I-ICG compounds. (B) ICG and I-ICG compounds and their corresponding absorbances and emission. The properties shown include synthetic yield (%), absorbance maxima (λ_{abs}, nm)/emission maxima (λ_{em}, nm), extinction coefficient (σ, M^{-1} cm^{-1}), and quantum yield (Φ_F, %) as measured in water. Reaction yields are indicated in parentheses.

that ICG's core structure can be modified, it is reasonable to presume that large changes to the structure would alter ICG's inherent tumor-targeting capability.[28] We hypothesize that a lower molecular weight iodine modification might better retain ICG's properties and open new avenues for its conversion into a radiopharmaceutical therapy or imaging agent.

The current uptake mechanism of ICG is only partially understood and is thought to be driven by solute carrier transporters (SLCs). These transporters are membrane-bound and are responsible for trafficking a wide range of small molecules into the cell.[29] One subset of SLCs is the organic anion transporter polypeptides (OATPs), which traffic organic anionic drugs and xenobiotics.[30,31] These include OATP1B1, OATP1B3, and OATP2B1 isoforms, which are expressed in the basolateral membrane of human hepatocytes, both healthy and cancerous, and have been proposed to play a role in ICG liver trafficking.[31,32] Previous experimental approaches in this area include the use of OATP inhibitors, which led to the suggestion that these transporters are involved in ICG hepatic clearance and the excretion of ICG.[33−38] The selectivity and retention of ICG in liver tumors may also be driven by decreased expression of multidrug resistance proteins, like MDR2, and/or disruption of cell polarity.[33,36]

Here, we design, synthesize, and test a series of iodinated ICG (I-ICG) analogs. To explore the tumor-targeting capability of these I-ICG analogs, we performed flow cytometry using commercial and patient-derived HCC and HB cancer cell lines. Additionally, we examined the molecular basis of ICG uptake via a CRISPR/dCas9 screen. We identify the putative ICG transporter OATP1B3, which was confirmed through the development of an overexpression cell line. This cell line was used to evaluate whether our I-ICG analogs could serve as substrates for this transporter. The lead compound from these studies was tested in mice bearing Hep3B and Huh-7 HCC tumor xenografts and patient-derived (PDX) HB xenografts to evaluate its biodistribution and clearance. This study presents a novel approach of placing iodine within the ICG scaffold and illustrates the effect that it has on the

https://doi.org/10.1021/acsmedchemlett.3c00213
ACS Med. Chem. Lett. 2023, 14, 1208−1215

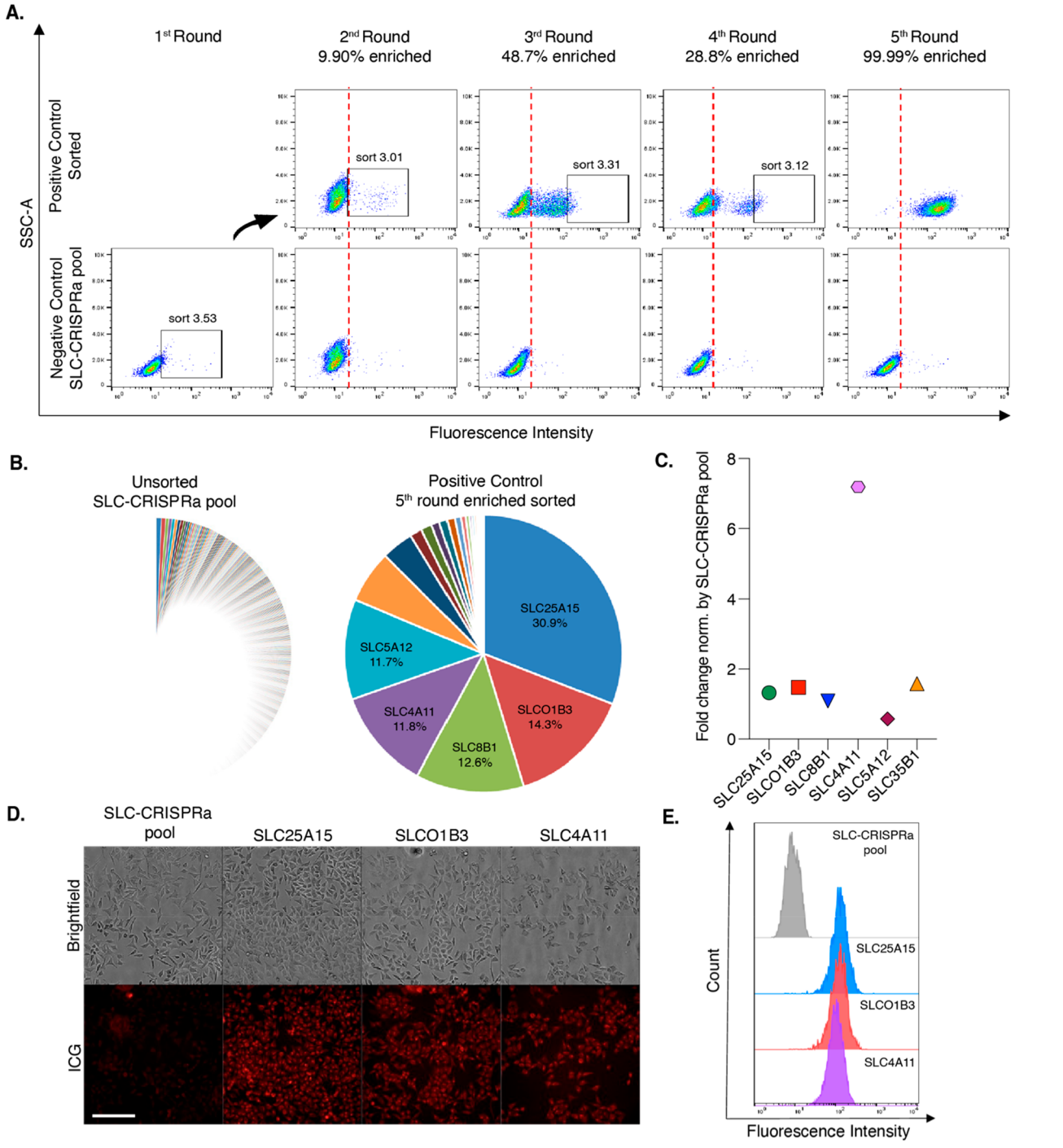

Figure 2. Identification of putative ICG transporters using a SLC-CRISPRa screen. (A) Increase of the ICG (10 μM) fluorescence intensity after SLC-CRISPRa pool enrichment. The top 3% brightest population was sorted every week until the sorted population up to the 5th round achieved 99.99% enhancement. (B) Pie chart demonstrating the proportion of highly enriched sgRNAs in the unsorted SLC-CRISPRa pool and the 5th round enriched population. NGS count results are presented as percentages for the top five targets. (C) Gene expression patterns of the top five SLC genes in the 5th round enriched population. The fold change was normalized to the SLC-CRISPRa pool. Clones exhibited high ICG uptake, as demonstrated through (D) microscopy and (E) flow cytometry. Scale bar represents 200 μm.

photophysical properties and biological uptake of heptamethine cyanines. Additionally, this study provides valuable information about alternative ICG structures that could be utilized for tumor-targeted radiopharmaceutical therapeutics and diagnostics or theranostics through the development of radioiodine ICG variants. Given that radiotherapy (e.g., ^{90}Y microsphere radioembolization and stereotactic radiotherapy) is often used for these cancers as part of standard-of-care, targeted radiopharmaceuticals could allow for accurate detection and post-treatment surveillance and expand our therapeutic repertoire.

In designing our I-ICG library, we focused on synthesizing compounds that not only incorporated small structural modifications to ICG's core but could potentially be

https://doi.org/10.1021/acsmedchemlett.3c00213
ACS Med. Chem. Lett. 2023, 14, 1208−1215

transformed into a radiotherapeutic in subsequent studies. Iodine-131 is routinely used alone or conjugated to tumor-selective molecules as a radiopharmaceutical therapy agent,[39−41] and iodine-124 can be used for positron emission tomography (PET) imaging.[42] Therefore, we synthesized iodine-containing ICG (I-ICG) analogs (Figure 1) using a synthetic methodology recently reported from our group (Figure 1A).[43] We focused on exploring whether installing iodine within the cyanine structure could improve the *in vivo* pharmacokinetic and liver tumor targeting properties of ICG.

After purification and characterization of all I-ICG derivatives, we explored their photophysical properties in water (Figure 1B) and phosphate-buffered saline (PBS) at pH 7.2 containing 10 mg/mL bovine serum albumin (BSA). The I-ICG analogs generally had more blue-shifted absorbance and emission maxima in both water and BSA/PBS in comparison to ICG (Figures 1B and S1−S5, Table S1). These results correlate with previous observations and are consistent with the fact that ICG has an extended π-system from the naphthalene groups, leading to a bathochromic shift in the absorbance maxima.[44,45] All compounds had higher extinction coefficients in water than BSA/PBS. All I-ICG compounds, including ICG, had moderate emission quantum yields ranging from 2−12% in water and 3−11% in BSA/PBS. The placement of the iodine on the indole ring had a strong effect on the emission quantum yields, with the 4-position exhibiting the greatest emission in water (12.3%). This enhanced quantum yield in comparison to ICG may indicate an improved fluorescence signal for *in vivo* imaging. Additionally, we evaluated the cLog*P* values of the compounds and found that the I-ICG compounds have values comparable to that of ICG and that the position of the iodine on the aryl ring does not affect the cLog*P* value (Table S1). These results could provide valuable information about the importance of iodine placement on the cyanine for potential photodynamic therapeutic (PDT) agents, which utilize a photosensitizing agent typically bearing heavy atoms like iodine to produce therapeutic singlet oxygen.[46]

We chose to examine ICG's cellular uptake in an unbiased manner by performing a systematic transporter screen using a CRISPRa activation library.[47] We examined 380 protein-encoded SLCs using a dCas9-VPR overexpression strategy. After five cycles of enrichment of the brightest ICG cell population using flow cytometry, six gene pools representing >80% of the total gene population were identified (Figure 2A−C). Of the six selected gene pools, SCL25A15, SLCO1B3, and SLC4A11 were shown to have the greatest fold change in gene expression after ICG treatment (Figure 2D and E). These SLCs are expressed in various tissues including the liver, kidneys, brain, heart, lungs, and intestines (Table S2). Of these genes, SLCO1B3 or OATP1B3 is most likely to play a role in ICG hepatic clearance or liver cancer uptake, as it is the only one expressed on the plasma membrane of liver cells and liver malignancies (Table S2). Furthermore, while not upregulated in liver cancer compared to healthy liver tissue, the high expression in all hepatocytes makes it a reasonable candidate for uptake in liver cancer cells.[48]

We then aimed to validate this target *in vitro* and test if OATP1B3 expression enhances the uptake of ICG and its analogs. We generated a stable OATP1B3 (SLCO1B3)-overexpressing cell line. This cell line was derived from HEK-293T kidney cells through transfection with the lentivirus SLCO1B3 OATP1c1.v1 with multiplicity of infection (MOI) ranging from 1−10. As a negative control, we also generated a cell line overexpressing SLC OATP1c1.v1, which was not implicated in ICG uptake in the CRISPRa screen. We validated the expression of OATP1B3 in this cell line through Western blot analysis and confirmed that there is an increased expression in the transfected HEK-293T cell lines in comparison to the lentiviral control and parent HEK-293T cell lines (Figure 3A). The uptake of ICG in our parent HEK-293T, OATP1B3 (MOI 10) HEK-293T, and the two liver cancer cell lines Hep3B and HepG2 was confirmed by confocal fluorescence microscopy (Figures 3B and S6) and flow cytometry (Figures 3C and S7−S10). Both methods confirmed that ICG uptake was greater in our OATP1B3 HEK-293T cells in comparison to the parent cell line and the other liver cancer cell lines. These results illustrate that OATP1B3 can mediate the uptake of ICG *in vitro*, and increased expression levels of this transporter result in greater ICG accumulation.

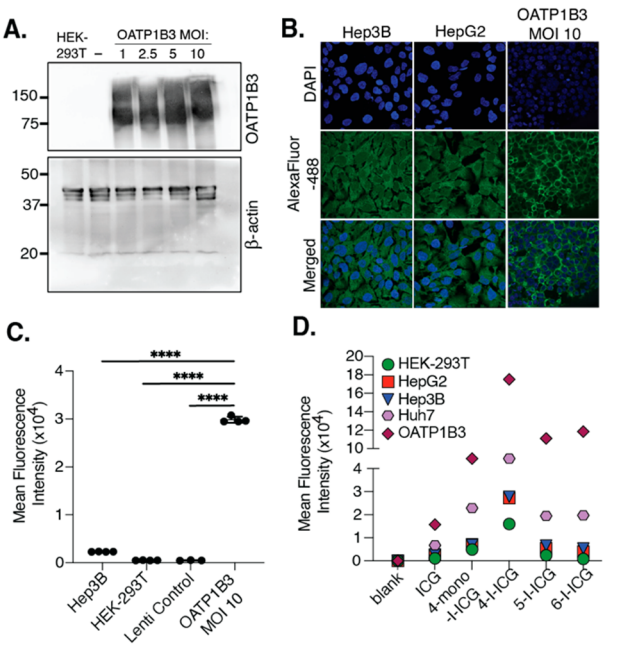

Figure 3. (A) Western blot depicting the expression of the protein OATP1B3 or β-actin in HEK-293T cells, HEK-293T cells infected with the lentivirus OATP1c1.v1 (−, Lenti control, MOI 10), or HEK-293T cells infected with an OATP1B3 lentivirus (MOI 1−10). (B) Confocal fluorescence microscope images of cells incubated with a primary anti-OATP1B3 antibody overnight (4 °C) and then for 1 h with an AlexaFluor-488-goat-antimouse IgG (H+L) at room temperature. Cells were stained with DAPI and imaged in Hank's buffered saline solution (HBSS) with a 63× oil-immersed lens. The full image is shown in Figure S6. (C) Flow cytometry of cells incubated with ICG (10 μM) for 1 h (at least three replicates per sample). Error bars represent the standard error of the mean. For statistical analysis, one-way ANOVA and Tukey's multiple comparisons were performed (n = 3 or 4, $F_{3,11}$ = 7389, ****$p \leq 0.0001$). (D) Mean fluorescence intensity of cells treated with 10 μM ICG or I-ICG compounds for 1 h.

To confirm the cell-type selectivity and mechanism of the I-ICG compounds, we treated OATP1B3 HEK-293T (MOI 10), HEK-293T, Hep3B (pediatric HCC), HepG2 (pediatric HB), and Huh-7 (adult HCC) cell lines with 10 μM of each compound for 1 h and then analyzed for fluorescence uptake via flow cytometry. We found that the greatest uptake for all I-

https://doi.org/10.1021/acsmedchemlett.3c00213
ACS Med. Chem. Lett. 2023, 14, 1208−1215

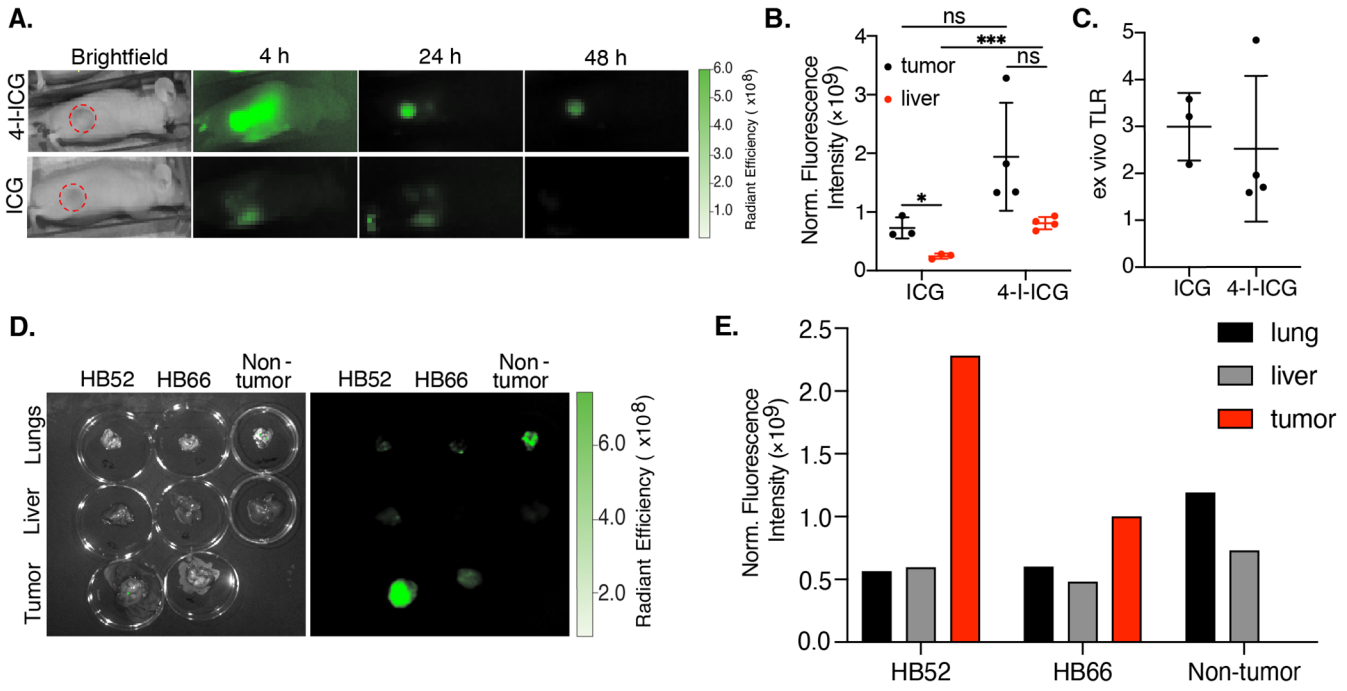

Figure 4. (A) Fluorescent *in vivo* images of Hep3B-tumor-bearing mice treated with 4-I-ICG (2 mg/kg) and ICG (2 mg/kg) at 4, 24, and 48 h postinjection. Tumors are highlighted in red circles. (B) *Ex vivo* analysis of tumors (black) and livers (red) of Hep3B-tumor-bearing mice treated with 4-I-ICG (2 mg/kg) and ICG (2 mg/kg) at 48 h postinjection. Background is determined by the fluorescence signal from the neck. (C) *Ex vivo* tumor-to-liver ratios (TLRs) of Hep3B-tumor-bearing mice treated with 4-I-ICG and ICG at 48 h postinjection. (D) Fluorescent *ex vivo* images of tumors, livers, and lungs of HB52-, HB66-, or non-tumor-bearing mice treated with 4-I-ICG (10 mg/kg) at 72 h postinjection. (E) *Ex vivo* analysis of lungs, liver, and tumor of HB52-, HB66-, or non-tumor-bearing mice treated with 4-I-ICG (10 mg/kg) at 72 h postinjection, $n = 1$. Data points are displayed as mean ± SD, and the p-values were evaluated by the Student's t test. $^{*}p \leq 0.05$, $^{***}p \leq 0.001$, ns is nonsignificant.

ICG analogs was observed in the OATP1B3 and Huh-7 cell lines. Additionally, the general trend was observed for all cell lines, 4-I-ICG ≫ 4-mono-I-ICG ≅ 5-I-ICG ≅ 6-I-ICG > ICG (Figure 3D and S11−S15). These results illustrate the importance of the placement of iodine on the indole for facilitating uptake and confirm that the I-ICG compounds can act as substrates for the OATP1B3 transporter.

Given that 4-I-ICG had the greatest and most selective uptake in a variety of liver cancer cells, we selected this compound for further validation *in vitro* with HB17 (pediatric HB patient-derived cell line). HepG2, HB17, and SH-SY5Y (neuroblastoma cell line with low ICG uptake) were exposed to 4-I-ICG or ICG for 1 h. The cells were then incubated with fresh media for 96 h and then analyzed for fluorescence uptake via flow cytometry (Figures S16−S19) or fluorescence microscopy (Figure S20). HepG2 and HB17 cells exhibit strong fluorescent signal with ICG or 4-I-ICG, while SH-SY5Y cells showed no fluorescence signal, confirming the liver cancer-cell selectivity of these compounds.

To test the tumor selectivity of 4-I-ICG *in vivo*, we performed optical imaging in two different HCC mouse models. Female athymic nude mice bearing either Hep3B or Huh-7 tumors were injected intravenously with 2 mg/kg 4-I-ICG or ICG and then the mice were imaged at 4, 24, and 48 h using an *in vivo* imaging system (IVIS). We observed tumor-to-background ratios (TBRs) of 5 and 2 for 4-I-ICG and ICG, respectively, in the Hep3B model (Figures 4A and S21). Comparable TBRs of ∼2 were observed in the Huh-7 model for both compounds (Figures S22 and S23). While the 4-I-ICG tumor signal was generally higher than that of ICG, the iodine compound also exhibited a higher liver signal, producing similar tumor-to-liver ratios (TLRs) in both tumor models (Figure S23). *Ex vivo* imaging at 48 h of the tumors and livers of each mouse confirmed that ICG and 4-I-ICG had comparable TLRs of around 2 or 3 for the Huh-7 and Hep3B models, respectively (Figures 4B/C and S24−S26). Overall, we saw lower fluorescence signals in the Huh-7 model for both ICG and 4-I-ICG than in the Hep3B model, indicating that the tumor model plays a role in the uptake of these dyes.

To test the selectivity of this analogue *in vivo* for HB, we performed optical imaging (IVIS) in two different orthotopic HB PDX models, HB52 and HB66. The sizes of the tumors were monitored using magnetic resonance imaging (MRI) until they reached 1 mm^3. The mice were injected intravenously with 10 mg/kg of 4-I-ICG and then imaged at 24, 48, and 72 h using IVIS (Figure S27). We observed *in vivo* clearance of 4-I-ICG in non-tumor-bearing mice at 48 h postinfusion. At 72 h, we appreciated *in vivo* clearance of one of the HB PDX models, HB66, while the signal was still present in the other model, HB52. *Ex vivo* analysis of both PDX models at 72 h postinjection showed strong signal in the tumor and minimal or no fluorescence in the liver (Figure 4D and E). Of note, the non-tumor-bearing mouse was shown to have nonspecific signal in the lungs at 72 h (Figure 4D and E). In both model systems, we observe selective uptake in the liver, with minimal uptake in other organs such as the kidneys, which is desirable given that kidney retention of current radiopharmaceutical agents is responsible for dose-limiting toxicity.[49] Given that the liver is a fairly radiotherapy-tolerant organ, as indicated by the current clinical use of ^{90}Y

https://doi.org/10.1021/acsmedchemlett.3c00213
ACS Med. Chem. Lett. 2023, 14, 1208−1215

radioembolization and external radiotherapy for therapy of HCC, we do not anticipate large adverse side effects with the radioiodine compound.[50] These *in vivo* studies highlight the ability of 4-I-ICG to target subcutaneous HCC and orthotopic HB tumors with high specificity.

Overall, we generated four new iodine containing ICG analogs that exhibited comparable photophysical and biological properties to the FGS agent ICG. We identified a likely uptake transporter for ICG, OATP1B3, through an unbiased CRISP-Ra screen, which may be responsible for the selectivity of ICG for liver tumors. Additionally, we concluded that our I-ICG analogs can also act as substrates for this transporter, indicating that we can retain the selectivity of these compounds through small structural modifications. This aspect could also be highly effective for targeting other tumor types with OATP1B3 overexpression, such as breast, prostate, or lung.[51] Future studies are still needed to address additional details of the export mechanism and the role of its potential disruption in solid tumor ICG retention. Out of the 4 new I-ICG compounds synthesized, we identified 4-I-ICG as the lead compound, as suggested by improved brightness and higher uptake in various liver cancer cell lines. This compound was tested in mice bearing Hep3B and Huh-7 HCC tumors as well as two orthotopic HB PDX tumor models, HB52 and HB66. *In vivo* and *ex vivo* analyses indicated that 4-I-ICG had better or comparable tumor uptake to ICG at the same dosing concentrations. These studies provide new ICG analogs for optical imaging/treatment purposes, as well as compounds with the potential to be developed as radiopharmaceutical theranostics. Such efforts may offer new, much needed, therapeutic and diagnostic options for patients with either HCC or HB.

■ ASSOCIATED CONTENT

Supporting Information

The Supporting Information is available free of charge at https://pubs.acs.org/doi/10.1021/acsmedchemlett.3c00213.

Additional experimental details, materials, and methods; NMR, HPLC, and HR-MS spectra; and biological experiments, including CRISPR, flow cytometry, confocal microscopy, and *in vivo* and *ex vivo* results (PDF)

■ AUTHOR INFORMATION

Corresponding Authors

Martin J. Schnermann − *Chemical Biology Laboratory, Center for Cancer Research, National Cancer Institute, National Institutes of Health, Frederick, Maryland 21702, United States;* orcid.org/0000-0002-0503-0116; Email: martin.schnermann@nih.gov

Sanjeev A. Vasudevan − *Divisions of Pediatric Surgery and Surgical Research, Michael E. DeBakey Department of Surgery, Pediatric Surgical Oncology Laboratory, Texas Children's Surgical Oncology Program and Liver Tumor Program, Dan L. Duncan Cancer Center, Baylor College of Medicine, Houston, Texas 77030, United States;* Email: sanjeevv@bcm.edu

Freddy E. Escorcia − *Molecular Imaging Branch, Center for Cancer Research, National Cancer Institute, National Institutes of Health, Bethesda, Maryland 20852, United States;* Email: freddy.escorcia@nih.gov

Young-Tae Chang − *Department of Chemistry, Pohang University of Science and Technology (POSTECH), Pohang, Gyeongbuk 37673, Republic of Korea;* orcid.org/0000-0002-1927-3688; Email: ytchang@postech.ac.kr

Authors

Sierra C. Marker − *Chemical Biology Laboratory, Center for Cancer Research, National Cancer Institute, National Institutes of Health, Frederick, Maryland 21702, United States*

Andres F. Espinoza − *Divisions of Pediatric Surgery and Surgical Research, Michael E. DeBakey Department of Surgery, Pediatric Surgical Oncology Laboratory, Texas Children's Surgical Oncology Program and Liver Tumor Program, Dan L. Duncan Cancer Center, Baylor College of Medicine, Houston, Texas 77030, United States*

A. Paden King − *Molecular Imaging Branch, Center for Cancer Research, National Cancer Institute, National Institutes of Health, Bethesda, Maryland 20852, United States*

Sarah E. Woodfield − *Divisions of Pediatric Surgery and Surgical Research, Michael E. DeBakey Department of Surgery, Pediatric Surgical Oncology Laboratory, Texas Children's Surgical Oncology Program and Liver Tumor Program, Dan L. Duncan Cancer Center, Baylor College of Medicine, Houston, Texas 77030, United States*

Roma H. Patel − *Divisions of Pediatric Surgery and Surgical Research, Michael E. DeBakey Department of Surgery, Pediatric Surgical Oncology Laboratory, Texas Children's Surgical Oncology Program and Liver Tumor Program, Dan L. Duncan Cancer Center, Baylor College of Medicine, Houston, Texas 77030, United States*

Kwamena Baidoo − *Molecular Imaging Branch, Center for Cancer Research, National Cancer Institute, National Institutes of Health, Bethesda, Maryland 20852, United States*

Meredith N. Nix − *Chemical Biology Laboratory, Center for Cancer Research, National Cancer Institute, National Institutes of Health, Frederick, Maryland 21702, United States*

Larissa Miasiro Ciaramicoli − *Department of Chemistry, Pohang University of Science and Technology (POSTECH), Pohang, Gyeongbuk 37673, Republic of Korea*

Complete contact information is available at: https://pubs.acs.org/10.1021/acsmedchemlett.3c00213

Author Contributions

[▽]These authors contributed equally. The manuscript was written through contributions of all authors. All authors have given approval to the final version of the manuscript.

Notes

The authors declare no competing financial interest.

■ ACKNOWLEDGMENTS

This work was supported by the Intramural Research Program of the National Institutes of Health (NIH), NCI-CCR (M.J.S), NIH ZIA [BC 011800 and BC 010891] (A.P.K., K.E.B., and F.E.E.), the Macy Easom Cancer Research Foundation Grant (S.A.V), a U.S. Department of Defense Career Development Award [CA201061] (S.E.W.), a Cancer Prevention and Research Institute of Texas (CPRIT) Multi-Investigator Research Award [RP180674] (S.A.V.), a Core Facility Support Grant from the CPRIT [RP170691] (S.A.V and S.E.W), a DOD Career Development Award [W81XWH-21-1-0396/

CA201061] (S.W), a Postdoctoral Research Associate Training (PRAT) fellowship from the National Institute of General Health and Medicine (NIGMS) [FI2GM146602-01] (S.C.M), and a Ruth L. Kirschstein Postdoctoral Individual National Research Service Award [1F32CA278313-01] (A.F.E). We thank Dr. Gary T. Pauly (National Cancer Institute) for assisting with the LC/MS and HPLC purification, Dr. Jeff Carrell (CCR-Frederick Flow Cytometry Core Laboratory), and Dr. Valentin Magidson (NCI-Optical Microscopy laboratory).

■ ABBREVIATIONS

ICG, indocyanine green; FGS, fluorescence-guided surgery; HCC, hepatocellular carcinoma; HB, hepatoblastoma; NIR, near-infrared; PDX, patient-derived xenograft; PBS, phosphate-buffered saline; BSA, bovine serum albumin; PDT, photodynamic therapy; SLC, solute carrier transporter; OAT, organic anion transporter; OATP, organic anion transporter polypeptide; MOI, multiplicity of infection; TBR, tumor-to-background ratio; TLR, tumor-to-liver ratio; MRI, magnetic resonance imaging; IVIS, *in vivo* imaging system

■ REFERENCES

(1) Llovet, J. M.; Kelley, R. K.; Villanueva, A.; Singal, A. G.; Pikarsky, E.; Roayaie, S.; Lencioni, R.; Koike, K.; Zucman-Rossi, J.; Finn, R. S. Hepatocellular carcinoma. *Nat. Rev. Dis Primers* **2021**, *7*, 6.

(2) Weeda, V. B.; Aronson, D. C.; Verheij, J.; Lamers, W. H. Is hepatocellular carcinoma the same disease in children and adults? Comparison of histology, molecular background, and treatment in pediatric and adult patients. *Pediatr Blood Cancer* **2019**, *66* (2), No. e27475.

(3) Allan, B. J.; Parikh, P. P.; Diaz, S.; Perez, E. A.; Neville, H. L.; Sola, J. E. Predictors of survival and incidence of hepatoblastoma in the paediatric population. *HPB (Oxford)* **2013**, *15* (10), 741−746.

(4) Watanabe, K. Current chemotherapeutic approaches for hepatoblastoma. *Int. J. Clin Oncol* **2013**, *18* (6), 955−961.

(5) Daher, S.; Massarwa, M.; Benson, A. A.; Khoury, T. Current and Future Treatment of Hepatocellular Carcinoma: An Updated Comprehensive Review. *J. Clin. Transl. Hepatol.* **2018**, *6* (1), 69−78.

(6) Ayllon Teran, D.; Gomez Beltran, O.; Ciria Bru, R.; Mateos Gonzalez, E.; Pena Rosa, M. J.; Luque Molina, A.; Lopez Cillero, P.; Briceno Delgado, J. Efficacy of neoadjuvant therapy and surgical rescue for locally advanced hepatoblastomas: 10 year single-center experience and literature review. *World J. Gastroenterol* **2014**, *20* (29), 10137−10143.

(7) Mieog, J. S. D.; Achterberg, F. B.; Zlitni, A.; Hutteman, M.; Burggraaf, J.; Swijnenburg, R. J.; Gioux, S.; Vahrmeijer, A. L. Fundamentals and developments in fluorescence-guided cancer surgery. *Nat. Rev. Clin Oncol* **2022**, *19* (1), 9−22.

(8) DSouza, A. V.; Lin, H.; Henderson, E. R.; Samkoe, K. S.; Pogue, B. W. Review of fluorescence guided surgery systems: identification of key performance capabilities beyond indocyanine green imaging. *J. Biomed Opt* **2016**, *21* (8), 080901.

(9) Nagaya, T.; Nakamura, Y. A.; Choyke, P. L.; Kobayashi, H. Fluorescence-Guided Surgery. *Front Oncol* **2017**, *7*, 314.

(10) Alander, J. T.; Kaartinen, I.; Laakso, A.; Patila, T.; Spillmann, T.; Tuchin, V. V.; Venermo, M.; Valisuo, P. A review of indocyanine green fluorescent imaging in surgery. *Int. J. Biomed Imaging* **2012**, *2012*, 940585.

(11) Yamada, Y.; Ohno, M.; Fujino, A.; Kanamori, Y.; Irie, R.; Yoshioka, T.; Miyazaki, O.; Uchida, H.; Fukuda, A.; Sakamoto, S.; Kasahara, M.; Matsumoto, K.; Fuchimoto, Y.; Hoshino, K.; Kuroda, T.; Hishiki, T. Fluorescence-Guided Surgery for Hepatoblastoma with Indocyanine Green. *Cancers (Basel)* **2019**, *11* (8), 1215.

(12) Nakaseko, Y.; Ishizawa, T.; Saiura, A. Fluorescence-guided surgery for liver tumors. *J. Surg Oncol* **2018**, *118* (2), 324−331.

(13) Gotoh, K.; Yamada, T.; Ishikawa, O.; Takahashi, H.; Eguchi, H.; Yano, M.; Ohigashi, H.; Tomita, Y.; Miyamoto, Y.; Imaoka, S. A novel image-guided surgery of hepatocellular carcinoma by indocyanine green fluorescence imaging navigation. *J. Surg Oncol* **2009**, *100* (1), 75−79.

(14) Ishizawa, T.; Fukushima, N.; Shibahara, J.; Masuda, K.; Tamura, S.; Aoki, T.; Hasegawa, K.; Beck, Y.; Fukayama, M.; Kokudo, N. Real-time identification of liver cancers by using indocyanine green fluorescent imaging. *Cancer* **2009**, *115* (11), 2491−2504.

(15) Tummers, Q. R.; Hoogstins, C. E.; Gaarenstroom, K. N.; de Kroon, C. D.; van Poelgeest, M. I.; Vuyk, J.; Bosse, T.; Smit, V. T.; van de Velde, C. J.; Cohen, A. F.; Low, P. S.; Burggraaf, J.; Vahrmeijer, A. L. Intraoperative imaging of folate receptor alpha positive ovarian and breast cancer using the tumor specific agent EC17. *Oncotarget* **2016**, *7* (22), 32144−32155.

(16) Whitlock, R. S.; Patel, K. R.; Yang, T.; Nguyen, H. N.; Masand, P.; Vasudevan, S. A. Pathologic correlation with near infrared-indocyanine green guided surgery for pediatric liver cancer. *J. Pediatr Surg* **2022**, *57* (4), 700−710.

(17) Lake, C. M.; Bondoc, A. J.; Dasgupta, R.; Jenkins, T. M.; Towbin, A. J.; Smith, E. A.; Alonso, M. H.; Geller, J. I.; Tiao, G. M. Indocyanine green is a sensitive adjunct in the identification and surgical management of local and metastatic hepatoblastoma. *Cancer Med.* **2021**, *10* (13), 4322−4343.

(18) Inagaki, Y.; Kokudo, T.; Kamiya, M.; Uno, S. N.; Sato, M.; Kaneko, J.; Kokudo, N.; Urano, Y.; Hasegawa, K. A novel liver-specific fluorescent anti-cancer drug delivery system using indocyanine green. *Sci. Rep* **2019**, *9*, 3044.

(19) Wu, J. B.; Shi, C.; Chu, G. C.; Xu, Q.; Zhang, Y.; Li, Q.; Yu, J. S.; Zhau, H. E.; Chung, L. W. Near-infrared fluorescence heptamethine carbocyanine dyes mediate imaging and targeted drug delivery for human brain tumor. *Biomaterials* **2015**, *67*, 1−10.

(20) Zhang, C.; Zhao, Y.; Zhang, H.; Chen, X.; Zhao, N.; Tan, D.; Zhang, H.; Shi, C. The Application of Heptamethine Cyanine Dye DZ-1 and Indocyanine Green for Imaging and Targeting in Xenograft Models of Hepatocellular Carcinoma. *Int. J. Mol. Sci.* **2017**, *18* (6), 1332.

(21) Zhao, N.; Zhang, C.; Zhao, Y.; Bai, B.; An, J.; Zhang, H.; Wu, J. B.; Shi, C. Optical imaging of gastric cancer with near-infrared heptamethine carbocyanine fluorescence dyes. *Oncotarget* **2016**, *7* (35), 57277−57289.

(22) James, N. S.; Chen, Y.; Joshi, P.; Ohulchanskyy, T. Y.; Ethirajan, M.; Henary, M.; Strekowsk, L.; Pandey, R. K. Evaluation of polymethine dyes as potential probes for near infrared fluorescence imaging of tumors: part - 1. *Theranostics* **2013**, *3* (9), 692−702.

(23) Usama, S. M.; Lin, C. M.; Burgess, K. On the Mechanisms of Uptake of Tumor-Seeking Cyanine Dyes. *Bioconjug Chem.* **2018**, *29* (11), 3886−3895.

(24) Usama, S. M.; Zhao, B.; Burgess, K. A Near-IR Fluorescent Dasatinib Derivative That Localizes in Cancer Cells. *Bioconjug Chem.* **2019**, *30* (4), 1175−1181.

(25) Jiang, Z.; Pflug, K.; Usama, S. M.; Kuai, D.; Yan, X.; Sitcheran, R.; Burgess, K. Cyanine-Gemcitabine Conjugates as Targeted Theranostic Agents for Glioblastoma Tumor Cells. *J. Med. Chem.* **2019**, *62* (20), 9236−9245.

(26) Cooper, E.; Choi, P. J.; Denny, W. A.; Jose, J.; Dragunow, M.; Park, T. I. The Use of Heptamethine Cyanine Dyes as Drug-Conjugate Systems in the Treatment of Primary and Metastatic Brain Tumors. *Front Oncol* **2021**, *11*, 654921.

(27) Choi, P. J.; Park, T. I. H.; Cooper, E.; Dragunow, M.; Denny, W. A.; Jose, J. Heptamethine Cyanine Dye Mediated Drug Delivery: Hype or Hope. *Bioconjug Chem.* **2020**, *31* (7), 1724−1739.

(28) Sevieri, M.; Silva, F.; Bonizzi, A.; Sitia, L.; Truffi, M.; Mazzucchelli, S.; Corsi, F. Indocyanine Green Nanoparticles: Are They Compelling for Cancer Treatment? *Front Chem.* **2020**, *8*, 535.

(29) Hediger, M. A.; Romero, M. F.; Peng, J. B.; Rolfs, A.; Takanaga, H.; Bruford, E. A. The ABCs of solute carriers: physiological, pathological and therapeutic implications of human membrane

https://doi.org/10.1021/acsmedchemlett.3c00213
ACS Med. Chem. Lett. 2023, 14, 1208−1215

transport proteinsIntroduction. *Pflugers Arch* **2004**, *447* (5), 465−468.
(30) Hagenbuch, B.; Meier, P. J. Organic anion transporting polypeptides of the OATP/ SLC21 family: phylogenetic classification as OATP/ SLCO superfamily, new nomenclature and molecular/ functional properties. *Pflugers Arch* **2004**, *447* (5), 653−665.
(31) Konig, J.; Cui, Y.; Nies, A. T.; Keppler, D. A novel human organic anion transporting polypeptide localized to the basolateral hepatocyte membrane. *Am. J. Physiol Gastrointest Liver Physiol* **2000**, *278* (1), G156−164.
(32) Cui, Y.; Konig, J.; Leier, I.; Buchholz, U.; Keppler, D. Hepatic uptake of bilirubin and its conjugates by the human organic anion transporter SLC21A6. *J. Biol. Chem.* **2001**, *276* (13), 9626−9630.
(33) Onda, N.; Kimura, M.; Yoshida, T.; Shibutani, M. Preferential tumor cellular uptake and retention of indocyanine green for in vivo tumor imaging. *Int. J. Cancer* **2016**, *139* (3), 673−682.
(34) de Graaf, W.; Hausler, S.; Heger, M.; van Ginhoven, T. M.; van Cappellen, G.; Bennink, R. J.; Kullak-Ublick, G. A.; Hesselmann, R.; van Gulik, T. M.; Stieger, B. Transporters involved in the hepatic uptake of (99m)Tc-mebrofenin and indocyanine green. *J. Hepatol* **2011**, *54* (4), 738−745.
(35) Shibasaki, Y.; Sakaguchi, T.; Hiraide, T.; Morita, Y.; Suzuki, A.; Baba, S.; Setou, M.; Konno, H. Expression of indocyanine green-related transporters in hepatocellular carcinoma. *J. Surg Res.* **2015**, *193* (2), 567−576.
(36) Huang, L.; Vore, M. Multidrug resistance p-glycoprotein 2 is essential for the biliary excretion of indocyanine green. *Drug Metab. Dispos.* **2001**, *29* (5), 634−637.
(37) Cusin, F.; Fernandes Azevedo, L.; Bonnaventure, P.; Desmeules, J.; Daali, Y.; Pastor, C. M. Hepatocyte Concentrations of Indocyanine Green Reflect Transfer Rates Across Membrane Transporters. *Basic Clin Pharmacol Toxicol* **2017**, *120* (2), 171−178.
(38) Shinohara, H.; Tanaka, A.; Kitai, T.; Yanabu, N.; Inomoto, T.; Satoh, S.; Hatano, E.; Yamaoka, Y.; Hirao, K. Direct measurement of hepatic indocyanine green clearance with near-infrared spectroscopy: separate evaluation of uptake and removal. *Hepatology* **1996**, *23* (1), 137−144.
(39) Luo, C.; Wu, G.; Huang, X.; Ma, Y.; Zhang, Y.; Song, Q.; Xie, M.; Sun, Y.; Huang, Y.; Huang, Z.; Hou, Y.; Xu, S.; Chen, J.; Li, X. Efficacy and safety of new anti-CD20 monoclonal antibodies versus rituximab for induction therapy of CD20(+) B-cell non-Hodgkin lymphomas: a systematic review and meta-analysis. *Sci. Rep* **2021**, *11*, 3255.
(40) Dhingra, J.; Halkar, R. I-131 MIBG therapy has been used as the first line therapy in pheochromocytoma. *J. Nucl. Med.* **2020**, *61*, 1452.
(41) Rodriguez-Santiago, S.; Cantu, E.; Wagner, R.; Savir-Baruch, B. Thyroid Cancer Therapy with 131I: A Comprehensive Review. *J. Nucl. Med.* **2016**, *57*, 1281.
(42) Phan, H. T.; Jager, P. L.; Paans, A. M.; Plukker, J. T.; Sturkenboom, M. G.; Sluiter, W. J.; Wolffenbuttel, B. H.; Dierckx, R. A.; Links, T. P. The diagnostic value of 124I-PET in patients with differentiated thyroid cancer. *Eur. J. Nucl. Med. Mol. Imaging* **2008**, *35* (5), 958−965.
(43) Usama, S. M.; Marker, S. C.; Li, D. H.; Caldwell, D. R.; Stroet, M.; Patel, N. L.; Tebo, A. G.; Hernot, S.; Kalen, J. D.; Schnermann, M. Method To Diversify Cyanine Chromophore Functionality Enables Improved Biomolecule Tracking and Intracellular Imaging. *J. Am. Chem. Soc.* **2023**, *145* (27), 14647−14659.
(44) Cosco, E. D.; Lim, I.; Sletten, E. M. Photophysical Properties of Indocyanine Green in the Shortwave Infrared Region. *ChemPhotoChem.* **2021**, *5* (8), 727−734.
(45) Stackova, L.; Muchova, E.; Russo, M.; Slavicek, P.; Stacko, P.; Klan, P. Deciphering the Structure-Property Relations in Substituted Heptamethine Cyanines. *J. Org. Chem.* **2020**, *85* (15), 9776−9790.
(46) Usama, S. M.; Thavornpradit, S.; Burgess, K. Optimized Heptamethine Cyanines for Photodynamic Therapy. *ACS Appl. Bio Mater.* **2018**, *1* (4), 1195−1205.
(47) Park, S. J.; Kim, B.; Choi, S.; Balasubramaniam, S.; Lee, S. C.; Lee, J. Y.; Kim, H. S.; Kim, J. Y.; Kim, J. J.; Lee, Y. A.; Kang, N.-Y.; Kim, J.-S.; Chang, Y.-T. Imaging inflammation using an activated macrophage probe with Slc18b1 as the activation-selective gating target. *Nat. Commun.* **2019**, *10*, 1111.
(48) Wlcek, K.; Svoboda, M.; Riha, J.; Zakaria, S.; Olszewski, U.; Dvorak, Z.; Sellner, F.; Ellinger, I.; Jager, W.; Thalhammer, T. The analysis of organic anion transporting polypeptide (OATP) mRNA and protein patterns in primary and metastatic liver cancer. *Cancer Biol. Ther* **2011**, *11* (9), 801−811.
(49) Strosberg, J. R.; Caplin, M. E.; Kunz, P. L.; Ruszniewski, P. B.; Bodei, L.; Hendifar, A.; Mittra, E.; Wolin, E. M.; Yao, J. C.; Pavel, M. E.; Grande, E.; Van Cutsem, E.; Seregni, E.; Duarte, H.; Gericke, G.; Bartalotta, A.; Mariani, M. F.; Demange, A.; Mutevelic, S.; Krenning, E. P. NETTER-1 Investigators. (177)Lu-Dotatate plus long-acting octreotide versus high-dose long-acting octreotide in patients with midgut neuroendocrine tumours (NETTER-1): final overall survival and long-term safety results from an open-label, randomised, controlled, phase 3 trial. *Lancet Oncol* **2021**, *22* (12), 1752−1763.
(50) Garin, E.; Tselikas, L.; Guiu, B.; Chalaye, J.; Edeline, J.; de Baere, T.; Assenat, E.; Tacher, V.; Robert, C.; Terroir-Cassou-Mounat, M.; Mariano-Goulart, D.; Amaddeo, G.; Palard, X.; Hollebecque, A.; Kafrouni, M.; Regnault, H.; Boudjema, K.; Grimaldi, S.; Fourcade, M.; Kobeiter, H.; Vibert, E.; Sourd, S. L.; Piron, L.; Sommacale, D.; Laffont, S.; Campillo-Gimenez, B.; Rolland, Y. Personalised versus standard dosimetry approach of selective internal radiation therapy in patients with locally advanced hepatocellular carcinoma (DOSISPHERE-01): a randomised, multicentre, open-label phase 2 trial. *Lancet Gastroenterol. Hepatol.* **2021**, *6* (1), 17−29.
(51) Buxhofer-Ausch, V.; Secky, L.; Wlcek, K.; Svoboda, M.; Kounnis, V.; Briasoulis, E.; Tzakos, A. G.; Jaeger, W.; Thalhammer, T. Tumor-specific expression of organic anion-transporting polypeptides: transporters as novel targets for cancer therapy. *J. Drug Deliv.* **2013**, *2013*, 863539.

https://doi.org/10.1021/acsmedchemlett.3c00213
ACS Med. Chem. Lett. 2023, 14, 1208−1215